Partial Lyapunov exponents in tangent space dynamics



1992 J. Phys. A: Math. Gen. 25 1915

(http://iopscience.iop.org/0305-4470/25/7/030)

J. Phys. A: Math. Gen. 25 (1992) 1915–1924. Printed in the UK

# Partial Lyapunov exponents in tangent space dynamics

A Campa, A Giansanti and A Tenenbaum

Dipartimento di Fisica, Università di Roma 'La Sapienza', Piazzale Aldo Moro 2, 00185 Roma, Italy

Received 23 July 1991, in final form 28 November 1991

**Abstract.** We have developed a new diagnostic tool for the analysis of the order-to-chaos transition: the partial Lyapunov exponents, defined through the dynamics in the tangent space. They allow the dynamics of single variables to be analysed, and are suitable for systems with several degrees of freedom. We have numerically simulated the dynamics of a model of five nonlinearly coupled oscillators; the partial Lyapunov exponents have been used to compute a characteristic coherence time for each degree of freedom. These quantities give information which is complementary to the usual statistical correlation times, and show that the high-frequency degrees of freedom, while losing their correlation during the order-to-chaos transition, may keep their coherence over long times.

## 1. Introduction

In systems with highly chaotic dynamics it is not expected to find qualitatively different behaviours among the different degrees of freedom: energy equipartition holds and all dynamical variables rapidly lose memory of their initial conditions. However, if the phase space also entails a region of highly ordered dynamics, there is usually a transition region where the system shows a mixed behaviour. In the transition region a partial chaoticity may induce differences in the dynamical evolution of the single degrees of freedom (DOFs). A detailed understanding of this particular regime can be important in real physical systems with a complex structure, in which the degree of chaos of a part of the system could significantly differ from that of another part.

The usual indicators of order and chaos either give information on the dynamics of the system as a whole (e.g. Lyapunov exponents [1], fractal dimensions [2], spectral entropy [3]) or are impractical for systems with many DOFs (Poincaré's maps, auto- and cross-correlation functions). Because of the need for tools able to predict the finite time behaviour of the single DOFs in a large system, we have elaborated a new diagnostic instrument, easy to compute and able to give insight into the short and medium time behaviour of each DOF in a complex structure. In this paper we describe the new tools, and implement them on a simple dynamical model which, however, retains an important feature of many complex systems: the presence of different characteristic frequencies, with values spanning a large range.

## 2. The model

Our model consists of a system of five nonlinearly coupled linear oscillators. The

0305-4470/92/071915+10$04.50  

Hamiltonian of the model is given by

$$H = \frac{1}{2}\sum_{i=1}^{5}(p_i^2 + \omega_i^2 q_i^2) + \frac{\alpha}{2}\sum_{i}^{1,5}\sum_{j(\neq i)}^{1,5} q_i^2 q_j^2. \tag{1}$$

The value of $\alpha$ can be modified at will rescaling the lengths; we have taken $\alpha = 1$. We have considered three cases, distinguished by the values of the frequencies $\omega_i$; they are shown in table 1. The choice of the values has been suggested by the purpose of having both resonant and non-resonant frequencies. In the no gap (NG) case, studied for comparison, the frequencies span a narrow range. In the other two cases, we studied the influence of a frequency gap on the dynamics of the various DOFs by multiplying $\omega_4$ and $\omega_5$ by 10 for small gap (SG) and by 30 for large gap (LG).

**Table 1.** Different versions of the model.

| Name | Symbol | $\omega_1$ | $\omega_2$ | $\omega_3$ | $\omega_4$ | $\omega_5$ |
|---|---|---|---|---|---|---|
| No gap | NG | 1 | $\frac{\pi}{2}$ | 2 | e | 3 |
| Small gap | SG | 1 | $\frac{\pi}{2}$ | 2 | 10e | 30 |
| Large gap | LG | 1 | $\frac{\pi}{2}$ | 2 | 30e | 90 |

We have numerically integrated both the equations of motion and the variation equations of motion with the central difference algorithm [4]. The initial conditions for the time evolution were generic; i.e. the energy was equally distributed on the five DOFs. The time step used in the integration was 1/50 of the shortest characteristic period $(2\pi/\omega_5)$ in each case. The second-order equations of motion are

$$\begin{aligned} \ddot{q}_i &= -\omega_i^2 q_i - 2\alpha \sum_{j(\neq i)}^{1,5} q_j^2 q_i \\ \ddot{p}_i &= -\left(\omega_i^2 + 2\alpha \sum_{j(\neq i)}^{1,5} q_j^2\right) p_i - 4\alpha \sum_{j(\neq i)}^{1,5} q_i q_j p_j \\ i &= 1,\ldots,5. \end{aligned} \tag{2}$$

The variation equations are usually written as first-order equations in the tangent space; if $\dot{x}_i = F_i(\{x_j\})$ are the Hamiltonian equations of motion, where $x_i$ is one of the $q_i$ or one of the $p_i$, then the equations of motion of the tangent space vector $y$ corresponding to the variation of $x$ have the following expression [1]:

$$\dot{y}_i = \sum_k \frac{\partial F_i(\{x_j\})}{\partial x_k} y_k \tag{3}$$

where the expression multiplying $y_k$ is computed along the trajectory $x(t)$. Here we write them in an equivalent form, more suitable for the numerical integration with

the central difference algorithm:

$$\begin{aligned}
\ddot{\xi}_i &= -\left(\omega_i^2 + 2\alpha \sum_{j(\neq i)}^{1,5} q_j^2(t)\right) \xi_i - 4\alpha \sum_{j(\neq i)}^{1,5} q_i(t) q_j(t) \xi_j \\
\ddot{\eta}_i &= -\left(\omega_i^2 + 2\alpha \sum_{j(\neq i)}^{1,5} q_j^2(t)\right) \eta_i - 4\alpha \xi_i \sum_{j(\neq i)}^{1,5} q_j(t) p_j(t) \\
&\quad - 4\alpha p_i(t) \sum_{j(\neq i)}^{1,5} q_j(t) \xi_j - 4\alpha q_i(t) \sum_{(j\neq i)}^{1,5} (q_j(t)\eta_j + p_j(t)\xi_j) \\
&\quad i = 1, \ldots, 5
\end{aligned} \tag{4}$$

where $(\xi_1, \ldots, \xi_5, \eta_1, \ldots, \eta_5) \equiv y$, with $\xi_i$ and $\eta_i$ corresponding to the variations of $q_i$ and $p_i$ respectively. The maximum Lyapunov exponent is given by

$$\lambda_M = \lim_{t \to +\infty} \lambda(t) \qquad \lambda(t) = \frac{1}{t} \ln \frac{|y(t)|}{|y(0)|} \tag{5}$$

where $y(0)$ is an initial vector taken randomly in the tangent space [1].

In order to have indicators referring to single DOFs we compute new quantities, which we call partial Lyapunov exponents (PLEs). Our definition is

$$\lambda_i \equiv \lim_{t \to +\infty} \lambda_i(t) \qquad \lambda_i(t) \equiv \frac{1}{2t} \ln \frac{\omega_i^2 \xi_i^2(t) + \eta_i^2(t)}{\omega_i^2 \xi_i^2(0) + \eta_i^2(0)} \qquad i \equiv 1, \ldots, 5. \tag{6}$$

It is necessary that at least one of the $\lambda_i$ is equal to $\lambda_M$; but, *a priori*, some of them could be smaller. However, since a generic initial vector in the tangent space will expand in modulus like $e^{\lambda_M t}$ when $t \to \infty$, with probability 1, one argues that $\lambda_i$, for all $i$, should also be equal to $\lambda_M$ with probability 1. Nevertheless, it is not to be expected that all $\lambda_i(t)$ are equal at finite times, and their differences are a relevant point of our investigation. We found that in the transition region between highly ordered and highly chaotic motions, for times three or four orders of magnitude higher than the characteristic periods of the oscillators, there are significant differences in the values of the $\lambda_i(t)$; we have used these differences to define a characteristic coherence time $\tau_i$ for each DOF. Let $\delta_i(t) = (\lambda(t) - \lambda_i(t))/\lambda_M$; then $\tau_i$ is defined as

$$\tau_i = \frac{1}{T} \int_0^T t \delta_i(t) \, dt \tag{7}$$

with $T$ such that both $\lambda(t)$ and $\lambda_i(t)$ have reached their asymptotic value $\lambda_M$.

## 3. Results

### *3.1. Maximum Lyapunov exponents*

We have studied our model at different values of $\epsilon$, the energy per DOF, or energy density. We have first computed the maximum Lyapunov exponents $\lambda_M$ to find out whether a transition in the dynamics takes place and the energy range in which this happens. In figure 1 we show $\lambda_M$ at different energy densities. From the change in the slope of $\lg(\lambda_M)$ (sharper in the cases with gap) it is evident that such a transition indeed takes place, and is located between $\epsilon = 0.9$ and $\epsilon = 1.0$. In fact, it has been shown [5] that such a change takes place at an energy value which can be interpreted as separating, in the phase space, dynamical regimes where diffusion is mainly chaotic (high energy) from dynamical regimes where diffusion is mainly of the Arnold type (low energy). This energy value has been called the strong stochasticity threshold [5]. Below this threshold the behaviour of the different versions is different, but the slopes are strongly positive; in particular, for the SG case, $\lambda_M$ changes by four orders of magnitude, passing from $\epsilon = 0.7$ to $\epsilon = 1.0$. Above the threshold the slopes of the graphs become small and the three cases have similar $\lambda_M$. At $\epsilon = 0.7$ we have compared the $\lambda_M$ of the different versions, as reported in table 2. One can see that the extension of the gap in the frequency spectrum is not correlated in a simple manner with the global chaos of the system, as measured by the value of $\lambda_M$.

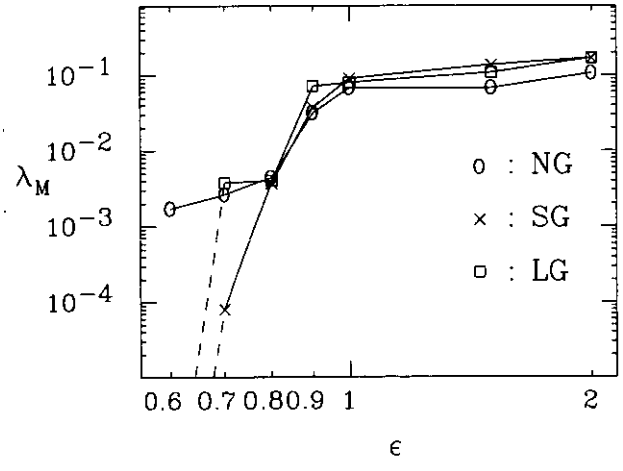


**Figure 1.** Maximum Lyapunov exponent against energy density for the NG, SG and LG cases. For $\epsilon = 0.6$, $\lambda_M$ is equal to zero in both the SG and LG cases.

### *3.2. Correlation functions*

We have collected in figures 2 and 3 the autocorrelation functions (ACFs) of the harmonic energies of the different DOFs for the SG case, at total energy densities of 0.7, 0.8, 0.9, and 1.0. In figures 2 and 3 only maxima and minima over groups of 100

**Table 2.** $\lambda_M$ for the different versions of the model; $\epsilon = 0.7$.

| Version | SG | NG | LG |
|---|---|---|---|
| $\lambda_M$ | $8.0 \times 10^{-5}$ | $2.6 \times 10^{-3}$ | $3.8 \times 10^{-3}$ |

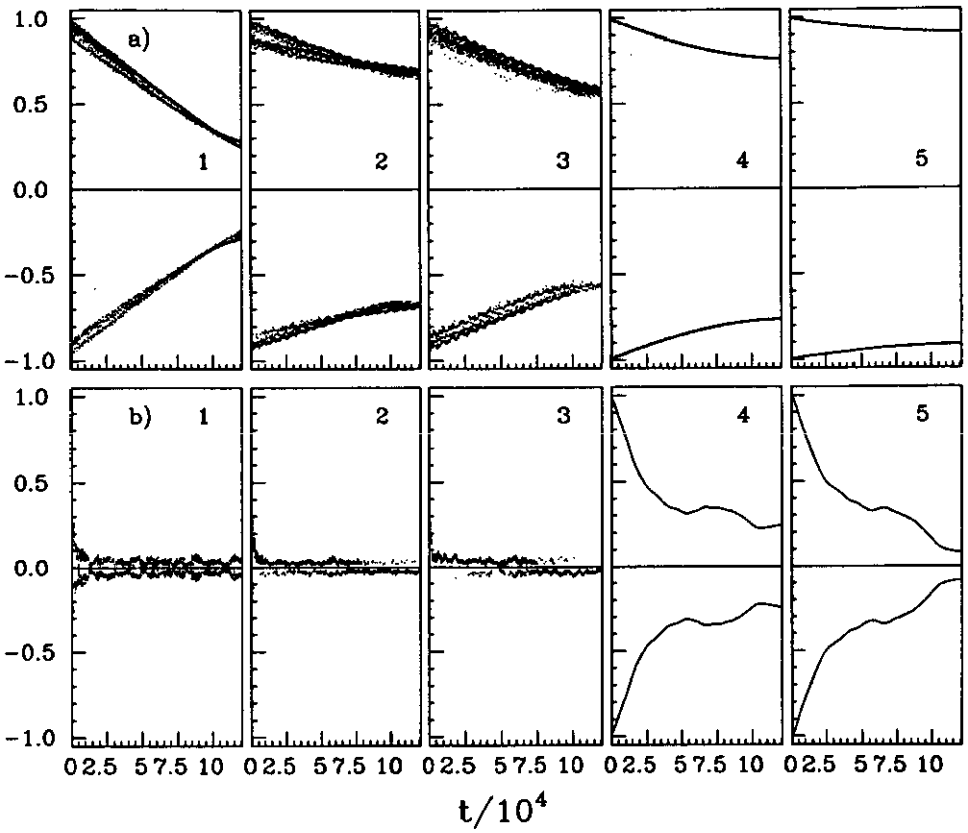


**Figure 2.** Autocorrelation functions for the harmonic energy of the five degrees of freedom, in the SG case, at two energy densities: (*a*) $\epsilon = 0.7$; (*b*) $\epsilon = 0.8$. The integer in each graph indicates the corresponding degree of freedom.

computed points were plotted, in order to have clear graphs over large times: in the case of an ACF rapidly oscillating around zero this appears as a symmetrical graph.

The ACFs have different decaying patterns: a clear distinction between the high- and low-frequency DOFs appears when the energy is increased. While the typical correlation times of all DOFs should decrease when the energy is raised, the rate of this decrease should be higher for the high-frequency DOFs than for the low-frequency ones. In fact, in the low-energy regime dominated by the presence of KAM tori, the high-frequency DOFs are expected to exhibit longer correlation times than the low-frequency DOFs [6]. For increasing energy a cross-over among DOFs should take place when the system reaches the phase space region where the measure of the KAM tori tends to zero and the space is filled with chaotic orbits: here the correlation time of each DOF is related to its characteristic period so that the high-frequency DOFs

should have shorter correlation times than the low-frequency ones.

Figures 2 and 3 show very clearly the expected cross-over in the energy density range 0.8–0.9. However, while the high-frequency ACFs (4 and 5) show, as expected, a monotonic decrease in the decay time, the low-frequency ones (1, 2 and 3) exhibit a peculiar rise in the decay time in the energy density window from $\epsilon = 0.8$ to $\epsilon = 0.9$; however, for energies higher than 1.0, the decay times of these functions also shorten. The ACFs have a complicated and diversified behaviour around the transition, reflecting the complex structure of the phase space. The behaviour of the ACFs for the LG case is similar to that shown here in the SG case, while in the NG case the ACFs do not show a clear distinction among DOFs.

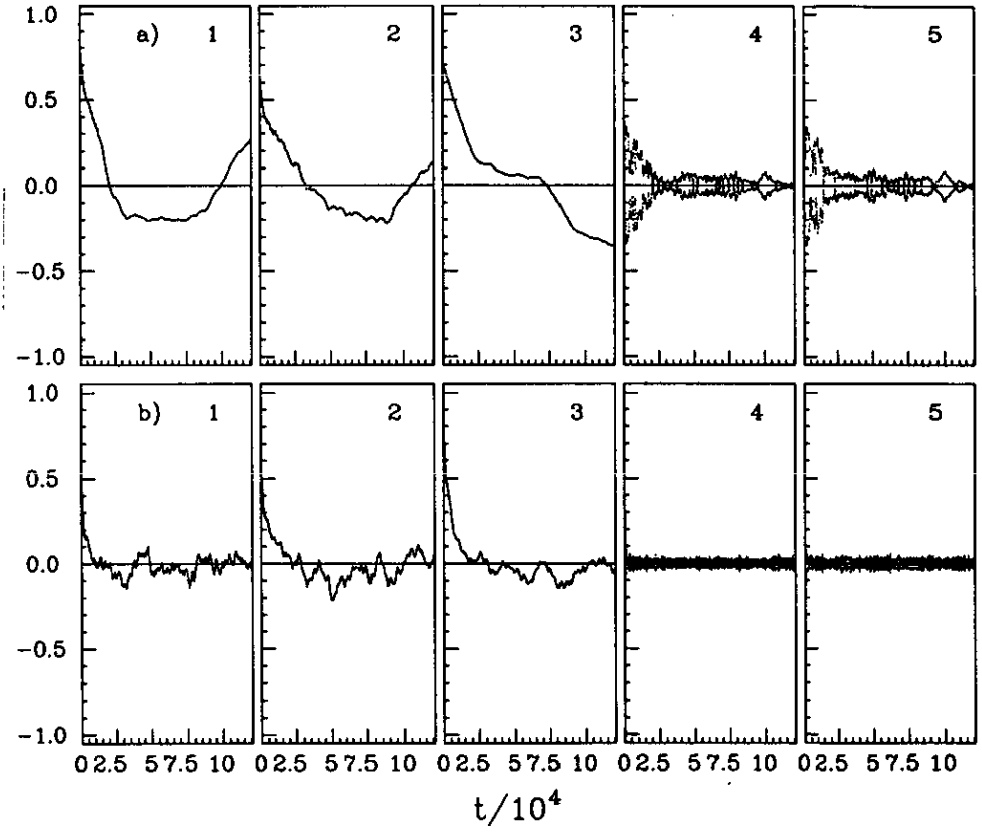


**Figure 3.** Same as in figure 2, for two further energy densities: (*a*) $\epsilon = 0.9$; (*b*) $\epsilon = 1.0$.

### *3.3. Partial Lyapunov exponents*

We have computed the PLEs for the five DOFs at various energies, encompassing the transition region individuated by $\lambda_M$. In figures 4 to 6 we show the graphs for the quantities $\delta_i(t)$, each one with five curves corresponding to the five DOFs, for three energies. It is clear that in the NG case the various curves behave in a similar way, although the fourth and fifth DOF show a higher degree of order at the beginning. On the other hand, in the cases with a gap the curves behave in very different ways in each graph; a group, corresponding to the DOFs with low characteristic frequencies,

oscillate around zero; the other group, corresponding to the high frequencies, decay to zero over large times. In figures 4 and 5 for the SG and LG cases there are peaks, in the curves related to the high-frequency DOFs, which are strictly correlated. Each peak appearing in a curve indicates that the corresponding DOF is just undergoing an intermittent phase of more coherent dynamics, which gives lower values of the corresponding $\lambda_i(t)$. Figure 6 shows that the peaks tend to disappear when the energy is raised.

**Table 3.** Coherence times of the degrees of freedom with higher frequency.

| $\epsilon$ | 0.7 | 0.8 | 0.9 | 1.0 | 2.0 |
|---|---|---|---|---|---|
| NG | | | | | |
| $\tau_4$ | 435 | 189 | 21 | 28 | 14 |
| $\tau_5$ | 557 | 336 | 57 | 34 | 16 |
| SG | | | | | |
| $\tau_4$ | 68 300 | 1630 | 182 | 64 | 35 |
| $\tau_5$ | 73 100 | 1740 | 192 | 69 | 37 |
| LG | | | | | |
| $\tau_4$ | 2080 | 2020 | 116 | 100 | 51 |
| $\tau_5$ | 2180 | 2110 | 121 | 104 | 54 |

In table 3 we report the values of the coherence times $\tau_i$ of the high-frequency DOFs at various energies. In each case $T \gg \tau_i$ in (7). The values computed for the low-frequency DOFs are less significant (and are therefore not given in table 3) because the variance of the integrand in (7) is very large. Nevertheless, we report that in the SG and LG cases they are much smaller than the $\tau_i$ of the high-frequency DOFs; they thus show a clear distinction between the dynamical behaviour of high-frequency and low-frequency DOFs. On the other hand, in the NG case, where we expect a more uniform behaviour from the various DOFs, we found that all the $\tau_i$ have the same order of magnitude.

The values of the $\tau_i$ given in table 3 show that while the general trend is of decreasing $\tau_i$ for increasing energy, the detailed behaviour of the DOFs manifests a more complicated pattern. Thus, for example, the $\tau_i$ for the SG case are sometimes larger and sometimes smaller than the corresponding $\tau_i$ of the LG case at the same energy. The $\tau_i$ in these two cases turn out to be roughly inversely proportional to $\lambda_M$, namely, $\tau_4$ and $\tau_5$ are given by $\tau_i = c_i/\lambda_M$, where $c_i$ seems to be independent of the energy and to depend only—but in a non-trivial way—on the $i$th frequency.

## 4. Discussion and comments

As already mentioned, in the SG and LG cases the ACFs show a characteristic behaviour: at low energy the functions corresponding to the high-frequency DOFs extend over times which are much larger than those of the functions corresponding to the low-frequency DOFs; when the energy is raised, a cross-over in the correlation times occurs. It is interesting to notice that a cross-over of characteristic relaxation times similar to that described here has been observed in the Fermi–Pasta–Ulam $\beta$ model [7]. However, it must also be noticed that it is often difficult to obtain a quantitative

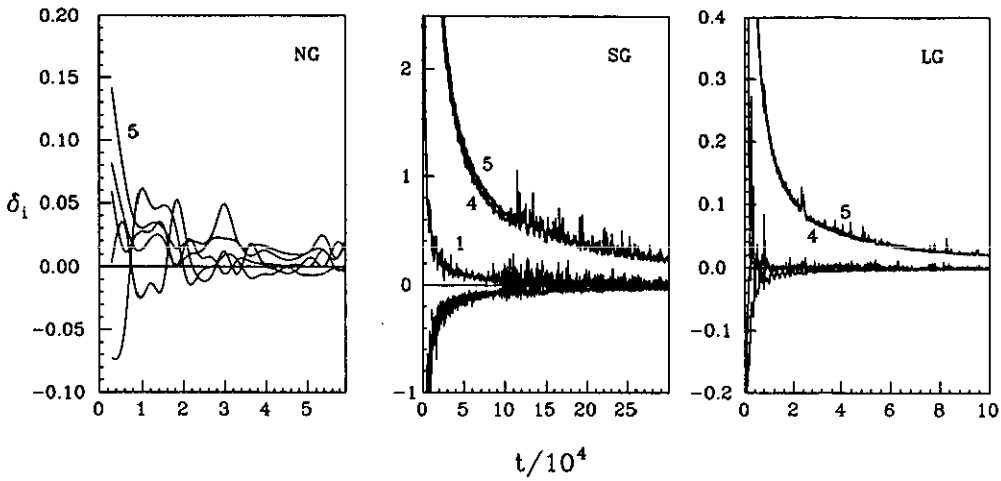


**Figure 4.** Functions $\delta_i(t)$ for the NG, SG and LG cases, for $\epsilon = 0.7$. The integers on the curves refer to the single degrees of freedom. Note that in this and in the next two figures some scales are different.

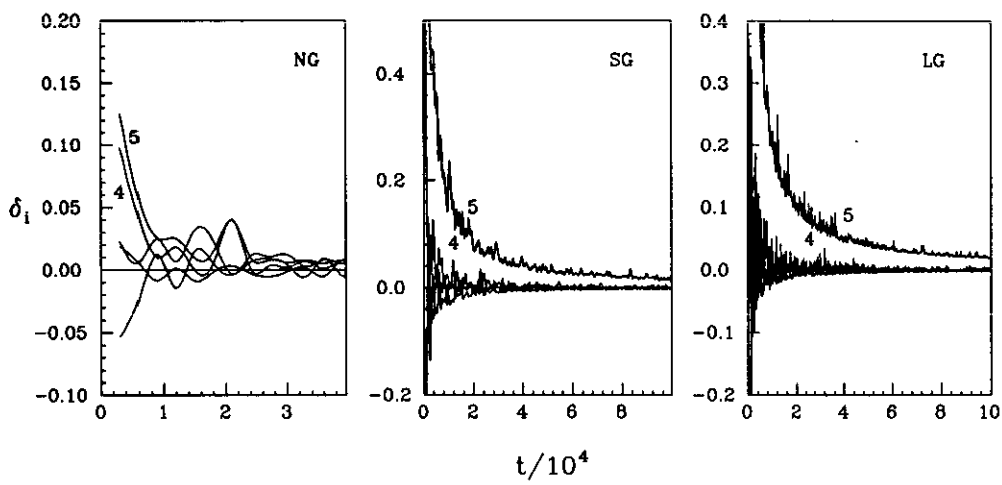


**Figure 5.** Same as in figure 4, for $\epsilon = 0.8$.

estimate of characteristic correlation times from the ACFs. It is evident, looking at figures 2 and 3, that the shape of the ACFs in most cases does not allow a characteristic decay time to be identified. Indeed, either the ACFs are correlated over times which are even greater than the whole simulation time (all DOFs at $\epsilon = 0.7$), or the structure is quite irregular (see, e.g., the fifth DOF at $\epsilon = 0.9$).

A comparison among the ACFs in the cases with gap gives a picture which is somehow in contradiction with the picture derived from the PLEs. Thus, while the PLEs show that the high-frequency DOFs on nearby trajectories diverge more slowly than the low-frequency DOFs, the corresponding ACFs at energies equal to and higher than 0.9 give a different indication, i.e. that the correlation is shorter for the high frequencies. Therefore, for energies above the cross-over region, the high-frequency DOFs have shorter correlation times but longer coherence times than the low-frequency DOFs.

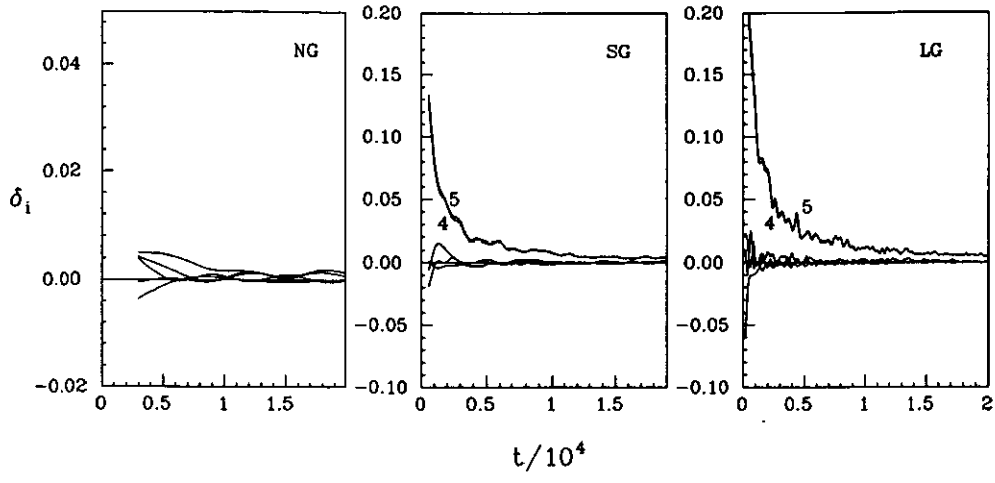


**Figure 6.** Same as in figure 4, for $\epsilon = 1.0$.

This complex situation may be understood in the following way. It is well known that the measure of the KAM tori on the hypersurface of constant energy decreases when the energy is raised. In the region where the stochastic sea coexists with residual KAM tori, the latter act as constraints for the trajectories of the system: they cannot bound undefinitely the trajectories (if the number of DOFs is greater than two), but they can force the system for a certain time into 'channels' running through them. In this situation, for generic initial conditions, the system will move in the stochastic sea; this will give short correlation times as shown by the ACFs at higher energies. However, due to the constraints exerted by the residual KAM tori, a trajectory starting from a slightly displaced initial condition—although equally stochastic—could be confined for a certain time near the first one. This behaviour is reflected in the existence of long coherence times for certain DOFs. Therefore, we can say that the PLEs and the coherence times $\tau_i$ measure the sensitiveness of each DOF to the presence of ordered portions (residual KAM tori or fragments of KAM tori) in the phase space; they thus give relevant information necessary to distinguish the short and medium time behaviour of the different DOFs of the system in the transition region. The fact that the coherence is maintained (mainly) in the high-frequency DOFs seems to be consistent with the Nekhoroshev theorem, from which one can derive [6] that the action variables corresponding to these DOFs are expected to have a slower divergence rate than the ones corresponding to the low-frequency DOFs. However, the last property has been derived for particular initial conditions, in which only one DOF with given characteristic frequency is initially excited. Since the energy exchange among nonlinear oscillators may depend strongly on their initial excitation, the extension of the result derived in [6] to our generic initial conditions may only be supposed.

The characteristic coherence times $\tau_i$ introduced by us single out the behaviour of a particular DOF in a complex situation like the one just depicted. We therefore believe that they can be particularly useful in studying dynamical states where the relevant DOFs behave in qualitatively different ways.

## References

[1] Benettin G, Galgani L and Strelcyn J M 1976 *Phys. Rev.* A **14** 2338
[2] Ott E 1981 *Rev. Mod. Phys.* **53** 655
[3] Livi R, Ruffo M, Sparpaglione M and Vulpiani A 1985 *Phys. Rev.* A **31** 1039
[4] Verlet L 1967 *Phys. Rev.* **159** 98
[5] Pettini M and Landolfi M 1990 *Phys. Rev.* A **41** 768
[6] Benettin G, Galgani L and Giorgilli A 1984 *Nature* **311** 444
[7] Pettini M and Cerruti-Sola M 1991 *Phys. Rev.* A **44** 975